energies

MDPI

Article

Active Disturbance Rejection Control Scheme for Reducing Mutual Current and Harmonics in Multi-Parallel Grid-Connected Inverters

Muhammad Saleem [1,2], Byoung-Sun Ko [1], Si-Hwan Kim [1], Sang-il Kim [3], Bhawani Shankar Chowdhry [4] and Rae-Young Kim [1,*]

1 Department of Electrical and Biomedical Engineering, Hanyang University, Seoul 04763, Korea; msmemon13@hanyang.ac.kr (M.S.); byoungsun1@hanyang.ac.kr (B.-S.K.); rlatis@hanyang.ac.kr (S.-H.K.)
2 Department of Electronic Engineering and Technology, Benazir Bhutto Shaheed University of Technology and Skills Development, Khairpur Mirs 66020, Pakistan
3 Department of Electrical Engineering, Daelim University College, Seoul 431715, Korea; sikim@daelim.ac.kr
4 Department of Electronics, Mehran University of Engineering and Technology, Jamshoro 76062, Pakistan; c.bhawani@ieee.org
* Correspondence: rykim@hanyang.ac.kr; Tel.: +82-2-2220-2897

Received: 31 October 2019; Accepted: 14 November 2019; Published: 15 November 2019

Abstract: With the increasing penetration of renewable energy sources into modern power systems, parallel inverters with LCL filters are commonly employed in the grid interface, giving rise to potential resonance problems. Among the different resonances, interactive resonance is triggered by interaction among inverters when different current references are applied to parallel inverters. It may also feature a mutual current that circulates among inverters instead of flowing into the grid and introduces harmonics or instability in the control system. In this paper, active disturbance rejection control based on a reduced-order extended state observer (RESO) was proposed for parallel inverters. With the proposed scheme, the interaction between inverters is considered as an exogenous disturbance caused by other parallel inverters, estimated by the RESO, and rejected by the controller. In the results, the mutual current and interactive harmonics, calculated via fast Fourier transform, were reduced with the proposed control scheme. Thus, the lower total harmonic distortion of each current was achieved. Additionally, the robust stability and less model-dependent control design are the other additive advantages over the derivative filtered capacitor voltage feedforward-based active damping using PI control. The simulation and real-time experimental results of the conventional and proposed scheme, obtained using the hardware-in-loop, were presented to verify the theoretical analysis under the similar and different current reference cases.

Keywords: active disturbance rejection control; circulating current; extended state observer; parallel grid-connected inverters; resonance

1. Introduction

1.1. Motivation and Incitement

Interest in distributed power-generation systems based on renewable energy sources (RESs) for sustainable development of the environment is growing. In this context, the pulse-width-modulated grid-connected inverter (GCI) has become the most widespread topology for delivering high-quality power from RESs to the grid. To attenuate the high-frequency switching harmonics generated by pulse-width modulation (PWM), the LCL filter has been increasingly adopted between the inverter and power grid [1].

The inherent resonance in the LCL filter can make the controller very complex and require a proper design with consideration of the grid impedance to avoid instability [2,3]. In renewable energy systems, it is common to connect multiple inverters in parallel with the grid to enhance the total generation capacity, leading to the resonance issue becoming more complex [4]. In such systems, internal, series, and interactive resonances have been observed [5]. Among them, interactive resonance, which is also known as parallel resonance, arises, owing to the mutual interaction between parallel GCIs operating under different current references [5–7].

1.2. Literature Review

Several studies have been conducted to mitigate the interactive resonance by introducing a virtual harmonic resistance [5], an active damper based on a high-bandwidth power converter [8], or capacitor current-based active damping [9–11]. The interactive resonance causes a mutual current—also known as an interactive current—which circulates among inverters instead of flowing into the grid. The relationship between the mutual current and the interactive resonance has been derived, and the adverse effects of the mutual current on the stability of parallel GCIs have been investigated [6,7,12]. However, in these studies, the harmonics introduced by the mutual current were not considered. In [13], the mutual current harmonics were investigated. The harmonics were divided into the low- and high-frequency components. However, the current-reference uncertainty in the RESs was not considered. In previous studies [14–16], the instability caused by the mutual current has been investigated under asynchronous PWM carriers or grid-impedance variation. However, the mutual current harmonics may increase the total harmonic distortion (THD) of inverter currents under operation with different references. The general LCL filter design guideline for preventing mutual current instability is provided in [17]. However, the dynamics of currents under different current references were not considered. Thus far, no effective solution for reducing the mutual current and harmonics under different current references in multi-parallel GCIs has been reported.

Active disturbance rejection control (ADRC), which is a disturbance observer-based control method, provides an active and effective way to handle complex/uncertain systems with minimal information about the system [18]. The ADRC estimates all the exogenous and endogenous disturbances, as a value called the lumped disturbance, in the system with the model-independent extended state observer (ESO), which is the main part of ADRC, and compensates them in the control law [19]. The reduction of the resonance harmonics for the LCL filter type GCI was investigated with ADRC in [20–22].

1.3. Contribution and Paper Organization

In this paper, a mutual current and resonance harmonics reduction scheme for multi-parallel GCIs with the reduced-order ESO (RESO)-based ADRC, irrespective of the current reference, was proposed. In addition, the common and mutual current expressions were derived with the proposed scheme. The interactive resonance among inverters was treated as an exogenous disturbance, estimated by RESO, and compensated by the proposed scheme. The damping of interactive and common resonances with the proposed method is explained by the frequency response method in the z-domain under different numbers of parallel inverters. The effective resonance damping resulted in greatly reduced mutual current and harmonics in the parallel grid-connected inverters. Furthermore, the stability of the system and disturbance rejection capabilities of the system were analyzed and compared with the conventional PI control using the derivative filter capacitor voltage feedforward-based active damping. To verify the performance of the proposed scheme, several experiments and harmonic analyses were performed for a system composed of two 3kVA inverters in parallel, to consider the worst case, using the real-time hardware-in-loop (HIL) simulation under similar and different reference cases.

The rest of the paper is organized as follows. The mathematical model of the multi-parallel GCI system with LCL filters is derived in Section 2. In Section 3, each element of the overall system with the proposed control scheme is explained, and the design guidelines for the RESO are provided. The common and mutual current expressions in relation to the current reference with the proposed

method are derived in Section 4. In Section 5, the resonance damping, stability analysis, and disturbance rejection capabilities of the proposed scheme are presented and compared with those of the conventional derivative filtered capacitor voltage feedforward-based active damping. A simulation and real-time experimental verification for validating the analysis performed in the preceding sections under different current-reference conditions are presented in Section 6. Conclusions are drawn in Section 7.

2. Mathematical Modeling of Multi-Parallel GCIs

The operation of multiple (n) parallel three-phase GCIs with LCL filters is shown in Figure 1. Each inverter is provided with a constant DC voltage V_{dci} ($i = 1, \ldots, n$). Z_{1i} and Z_{2i} represent the inverter- and grid-side inductor impedances, respectively, Z_{3i} represents the filter capacitance impedances, and Z_g represents the inductive grid impedance. The inverter-side currents and voltages are represented by i_i and v_i, respectively. e_g represents the ideal and balanced grid voltage, and v_{pcc} represents the voltage at the point of common coupling (PCC). The inverter parameters are assumed to be identical, i.e.,

$$Z_{1i} = sL_1,\ Z_{2i} = sL_2,\ Z_{3i} = \frac{1}{sC_3}, V_{dci} = V_{dc} \tag{1}$$

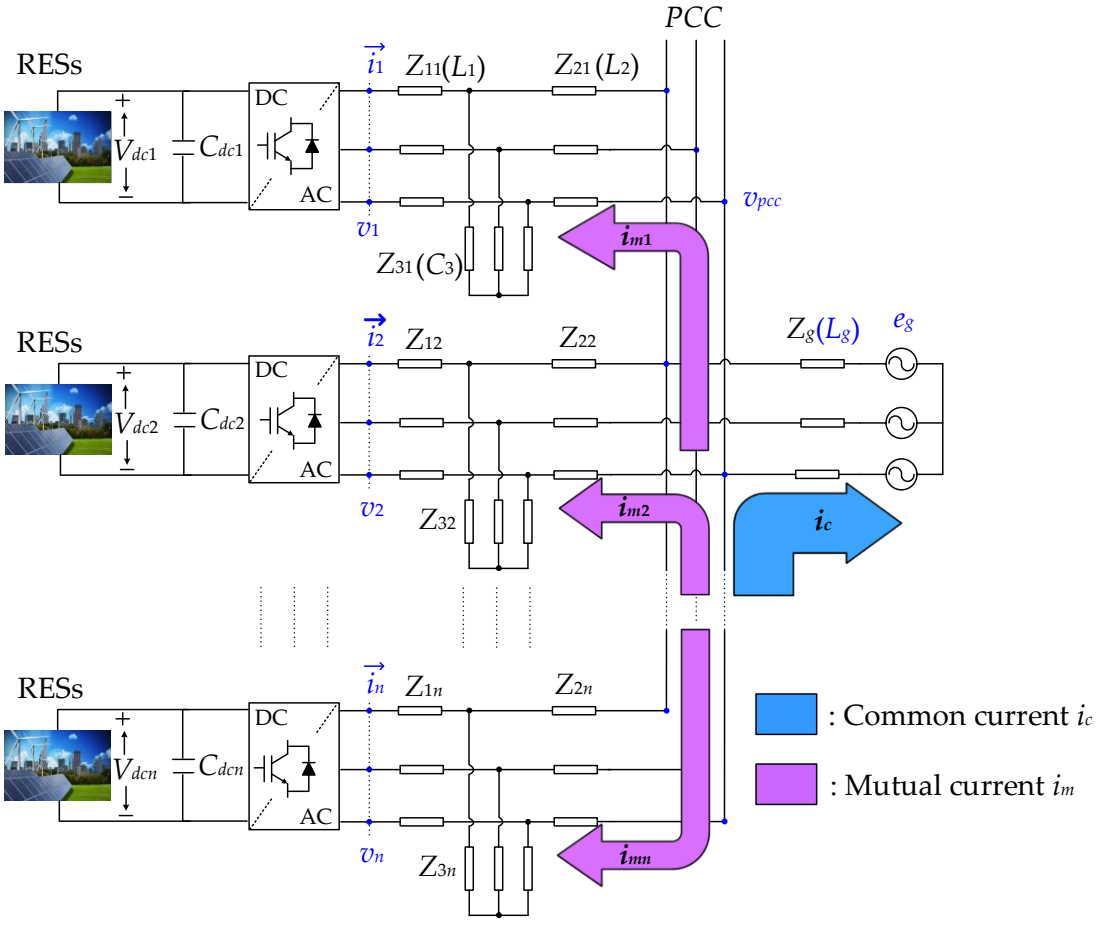

Figure 1. Renewable energy sources (RESs)-based LCL filter-type multi-parallel three-phase grid-connected inverters (GCIs).

Each current i_i makes ($n - 1$) minor contributions to the other j inverters and one major contribution to the grid. The minor contribution is defined as mutual currents i_{mj} ($j = 1, \ldots, n$ and $j \neq i$), which circulate among other inverters. The major contribution is defined as a common current i_c. The

multi-parallel GCIs is a multi-input-multi-output system [23]. The relationship between the output currents i_i and input voltages v_i for multi-parallel GCIs can be derived as

$$\begin{pmatrix} i_1(s) \\ i_2(s) \\ \cdots \\ i_n(s) \end{pmatrix} = Y(s) \cdot \begin{pmatrix} v_1(s) \\ v_2(s) \\ \cdots \\ v_n(s) \end{pmatrix} = \begin{pmatrix} Y_{11}(s) & Y_{12}(s) & \cdots & Y_{1n}(s) \\ Y_{21}(s) & Y_{22}(s) & \cdots & Y_{2n}(s) \\ \cdots & \cdots & \cdots & \cdots \\ Y_{n1}(s) & Y_{n2}(s) & \cdots & Y_{nn}(s) \end{pmatrix} \cdot \begin{pmatrix} v_1(s) \\ v_2(s) \\ \cdots \\ v_n(s) \end{pmatrix} \tag{2}$$

where $Y(s)$ is the $n \times n$ admittance matrix of the system. In Equation (2), the impact of each inverter's own voltage $v_i(s)$ on its own current $i_i(s)$ is represented by diagonal elements $Y_{ii}(s)$, and the impact of other inverter voltages $v_j(s)$ on the current $i_i(s)$ is represented by non-diagonal elements $Y_{ij}(s)$. For an n parallel inverter system, an index i corresponds to the inverter under consideration, and an index j corresponds to each of the remaining $(n-1)$ inverter modules. All the diagonal elements are the same when we assume identical parameters for each inverter. Similarly, all non-diagonal elements are the same. By using the superposition principle, the diagonal and non-diagonal elements can be derived as [6,7,12]

$$\begin{aligned} Y_{ii}(s) &= \tfrac{n-1}{n} \cdot G_{plant}(s) + \tfrac{1}{n} \cdot G_{coupling}(s) \\ Y_{ij}(s) &= -\tfrac{1}{n} \cdot G_{plant}(s) + \tfrac{1}{n} \cdot G_{coupling}(s) \end{aligned} \tag{3}$$

where $G_{plant}(s)$ and $G_{coupling}(s)$ represent the LCL filter transfer function and grid impedance coupling transfer function, respectively.

$$\begin{aligned} G_{plant}(s) &= \tfrac{1}{L_1 L_2 C_3} \cdot \tfrac{L_2 C_3 \cdot s^2 + 1}{s\left(s^2 + \omega_{res}^2\right)} \\ G_{coupling}(s) &= \tfrac{1}{L_1\left(L_2 + nL_g\right)C_3} \cdot \tfrac{\left(L_2 + nL_g\right)C_3 \cdot s^2 + 1}{s\left(s^2 + \omega_{res1}^2\right)} \end{aligned} \tag{4}$$

Here, ω_{res} and ω_{res1} are defined as the interactive and common resonance frequencies, respectively.

$$\begin{aligned} \omega_{res} &= \sqrt{(L_1 + L_2)/L_1 L_2 C_3} \\ \omega_{res1} &= \sqrt{\left(L_1 + L_2 + nL_g\right)/L_1\left(L_2 + nL_g\right)C_3} \end{aligned} \tag{5}$$

From Equation (4), it can be easily seen that G_{plant} (s) and $G_{coupling}$ (s) become identical when L_g is zero, and accordingly, all the non-diagonal elements $Y_{ij}(s)$ become zero. Consequently, no interaction among inverters is observed [7]. However, when L_g is not zero, each inverter interacts with not only a grid but also the other inverters. In this case, the current $i_i(s)$ can be expressed as

$$i_i(s) = \sum_{j=1, j \neq i}^{n} i_{mj}(s) + i_c(s) = i_{ms}(s) + i_c(s) \tag{6}$$

where $i_{ms}(s)$ represents the sum of $(n-1)$ contributions of current $i_i(s)$ as a mutual current.

From Equation (2), $i_i(s)$ can be expressed as

$$i_i(s) = Y_{ii}(s) \cdot v_i(s) + \sum_{j=1, j \neq i}^{n} Y_{ij}(s) \cdot v_j(s) \tag{7}$$

From Equations (3), (6) and (7), the currents $i_{ms}(s)$ and $i_c(s)$ are derived as

$$\begin{aligned} i_{ms}(s) &= \tfrac{1}{n} G_{plant}(s)\left((n-1)v_i(s) - \sum_{j=1, j \neq i}^{n} v_j(s)\right) \\ i_c(s) &= \tfrac{1}{n} G_{coupling}(s)\left(v_i(s) + \sum_{j=1, j \neq i}^{n} v_j(s)\right) \end{aligned} \tag{8}$$

Note that $i_{ms}(s)$ depends on $G_{plant}(s)$ and becomes zero when all the inverter voltages are the same. After applying a *abc to dq* transformation to Equation (8), we obtain

$$\begin{aligned} i_{ms}^{dq}(s) &= \tfrac{1}{n} G_{plant}^{dq}(s)\left((n-1)v_i^{dq}(s) - \sum_{j=1,j\neq i}^{n} v_j^{dq}(s)\right) \pm \omega_g(L_1+L_2) i_{ms}^{qd}(s) \\ i_c^{dq}(s) &= \tfrac{1}{n} G_{coupliong}^{dq}(s)\left(v_i^{dq}(s) + \sum_{j=1,j\neq i}^{n} v_j^{dq}(s)\right) \pm \omega_g(L_1+L_2) i_c^{qd}(s) \end{aligned} \tag{9}$$

where $i_{ms}^{dq}(s)$ and $i_c^{dq}(s)$ are the dq components of currents $i_{ms}(s)$ and $i_c(s)$, respectively. Similarly, $v_i^{dq}(s)$ and $v_j^{dq}(s)$ are the dq components of voltages $v_i(s)$ and $v_j(s)$, respectively. The term $\omega_g(L_1{+}L_2)i_{ms}^{qd}(s)$ in the mutual current and $\omega_g(L_1{+}L_2)i_c^{qd}(s)$ in the common current represent the coupling effect between the respective dq variables. The transfer functions $G_{plant}^{dq}(s)$ and $G_{coupling}^{dq}(s)$ can be derived as

$$\begin{aligned} G_{plant}^{dq}(s) &= \frac{\left(L_2C_3s^2 - {\omega_g}^2L_2C_3 + 1\right)}{L_1L_2C_3\left(s^3 + \omega_{res}^2 s - {\omega_g}^2\right)} \\ G_{coupling}^{dq}(s) &= \frac{\left((L_2+nL_g)C_3s^2 - {\omega_g}^2(L_2+nL_g)C_3 + 1\right)}{L_1\left(L_2+nL_g\right)C_3\left(s^3 + \omega_{res1}^2 s - {\omega_g}^2\right)} \end{aligned} \tag{10}$$

where ω_g represents the grid frequency. All the parameters of the multi-parallel GCIs are presented in Table 1.

Table 1. System parameters of multi-parallel GCIs.

Parameter	Symbol	Value
Grid Voltage	e_g	$120V_{rms}$
Grid Frequency	ω_g	60 Hz
Power Rating	P_{iref}	3 kVA
Reactive Power Rating	Q_{iref}	0
DC Voltage	V_{dc}	400 V
Switching Frequency	f_{sw}	20 kHz
Sampling Frequency	f_s	20 kHz
Inverter-side Impedance	L_1	2.5 mH
Grid-side Impedance	L_2	1 mH
Filter Capacitance	C_3	4 μF
Grid Impedance	$Z_g(L_g)$	1 mH

3. Proposed Mutual Current Reduction Scheme

The overall system with the proposed RESO-based ADRC current control scheme for the multi-parallel three-phase GCIs is shown in Figure 2, where i_i^d and i_i^q represent the d and q components of i_i, respectively, and v_{gi}^d and v_{gi}^q represent the d and q components of v_{pcc}, respectively. The current i_i, which is influenced by all the other j inverters voltages v_j, is chosen as a feedback to the current control. The v_{pcc} is sensed only for the current and voltage synchronization around ω_g with the phase-locked loop (PLL). The current references i_{iref}^d and i_{iref}^q are generated independently by the active power P_{iref} and reactive power Q_{iref} references applied to each inverter, respectively. The six-pulse IGBT gate signals s_{i1} to s_{i6} are also generated separately for each inverter by applying space-vector modulation (SVM) to the control signals u_i^{abc} provided by each RESO-based ADRC control block after performing inverse dq transformation on control signals u_i^d and u_i^q. For i_i^d and i_i^q regulations, the inverters have decentralized control blocks with identical structures and no communication.

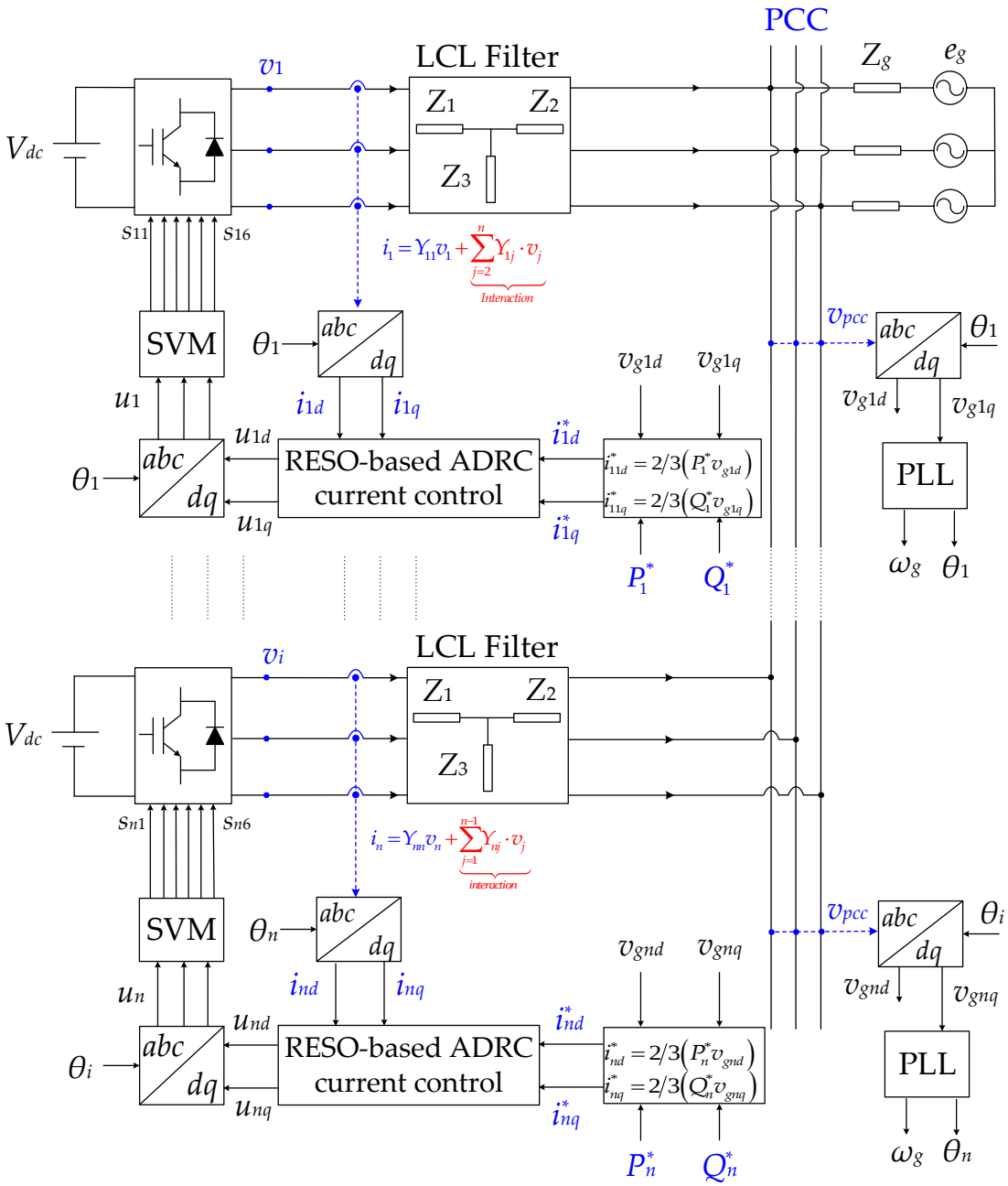

Figure 2. Overall system with the proposed reduced-order extended state observer (RESO)-based active disturbance rejection control (ADRC) current control scheme.

The detailed diagram with the proposed control scheme from Figure 2 for any inverter i in the z-domain is shown in Figure 3. In this paper, only $i_i^d(z)$ regulation is explained, for simplicity, and a similar configuration for $i_i^q(z)$ regulation is adopted. The $i_i^d(z)$ is compared with i_{iref}^d, followed by proportional control with the gain K_p selected according to the required performance of the control. The estimated lumped disturbance z_{2i}^d calculated by the RESO is subtracted to compensate for the exogenous disturbance, i.e., the effect of the sum of the other j inverters voltages. In the result, the control signal $u_i^d(z)$ is generated after dividing by the turning parameter b, which is equal to $1/L_1$. The z^{-1} represents an inherent delay caused by computation and the PWM update, and the inverter is simplified as a linear amplifier with gain K_{PWM}. Finally, the $v_i^d(z)$ is generated. Similarly, $v_j^d(z)$ is generated by $i_j^d(z)$ current regulation of any other j inverters. The control plant, which comprises multi-parallel GCIs in the discrete time domain is represented as a block-diagram according to Equation

(9). With the consideration of the zero-order-hold (ZOH) effect in Figure 3, the discrete representations of $G^d_{plant}(s)$ and $G^d_{coupling}(s)$ are given as [24]

$$\begin{aligned} G^d_{plant}(z) &= \left(1-z^{-1}\right)\mathcal{Z}\left[\mathcal{L}^{-1}\left[\frac{G^d_{plant}(s)}{s}\right]\right] \\ G^d_{coupling}(z) &= \left(1-z^{-1}\right)\mathcal{Z}\left[\mathcal{L}^{-1}\left[\frac{G^d_{coupling}(s)}{s}\right]\right] \end{aligned} \tag{11}$$

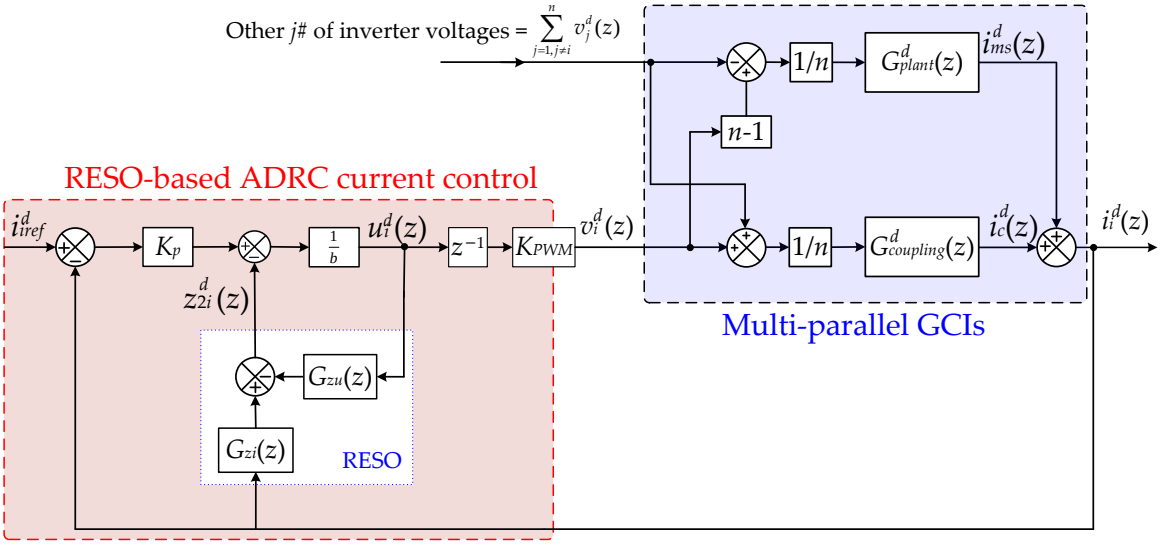

Figure 3. Overall system with the proposed RESO-based ADRC current control scheme. Proposed RESO-based first-order ADRC current control scheme for multi-parallel GCIs.

With the proposed scheme, the interaction influence of other inverters on each current can be treated as an exogenous disturbance, whereas the coupling effect between the dq variables is treated as an endogenous disturbance.

In general, the state-space model of a first-order time-delayed system with an extended state can be represented as

$$\begin{aligned} \begin{bmatrix} \dot{x}_1(t) \\ \dot{x}_2(t) \end{bmatrix} &= \begin{bmatrix} 0 & 1 \\ 0 & 0 \end{bmatrix}\begin{bmatrix} x_1(t) \\ x_2(t) \end{bmatrix} + \begin{bmatrix} b \\ 0 \end{bmatrix}u_c(t-T_s) + \begin{bmatrix} 0 \\ 1 \end{bmatrix}f(t) \\ y(t) &= \begin{bmatrix} 1 & 0 \end{bmatrix}\begin{bmatrix} x_1(t) \\ x_2(t) \end{bmatrix} \end{aligned} \tag{12}$$

where $x_1(t)$ and $x_2(t)$ represent the system states and $y(t)$ is the output of the system. b is the control gain parameter, $u_c(t-T_s)$ is the control input with a time delay of sampling time T_s, and $f(t)$ represents the lumped disturbance in the system.

Generally, the second-order ESO, which is the core part of first-order ADRC, is constructed as

$$\begin{bmatrix} \dot{z}_1(t) \\ \dot{z}_2(t) \end{bmatrix} = \begin{bmatrix} 0 & 1 \\ 0 & 0 \end{bmatrix}\begin{bmatrix} z_1(t) \\ z_2(t) \end{bmatrix} + \begin{bmatrix} b \\ 0 \end{bmatrix}u_c(t-T_s) + \begin{bmatrix} \beta_1 \\ \beta_2 \end{bmatrix}(x_1(t)-z_1(t)) \tag{13}$$

where $z_1(t)$ and $z_2(t)$ are the estimated values of $x_1(t)$ and $x_2(t)$, respectively, and $\begin{bmatrix} \beta_1 \\ \beta_2 \end{bmatrix}$ is the gain matrix of the ESO.

Assuming that $x_1(t)$ is known through measurement, Equation (13) can be reduced to an estimation of $z_2(t)$:

$$\dot{z}_2(t) = [0]z_2(t) + [0]u_c(t - T_s) + \beta_2(x_2(t) - z_2(t)) \tag{14}$$

Using Equation (12), we can rewrite Equation (14) as

$$\dot{z}_2(t) = \beta_2\Big(\dot{y}_1(t) - bu_c(t - T_s) - z_2(t)\Big) \tag{15}$$

where the observer gain β_2 is selected as an observer bandwidth ω_o.

After applying the Laplace transform to Equation (15) and separating the two terms $u_c(s)$ and $y(s)$, the output-to-estimation transfer function $G_{zy}(s)$ and the control-to-estimation transfer function $G_{zu}(s)$ are derived as

$$\begin{aligned} G_{zy}(s) &= \frac{z_2(s)}{y(s)} = \frac{\beta_2 s}{(s+\beta_2)} \\ G_{zu}(s) &= \frac{z_2(s)}{u_c(s)} = \frac{\beta_2 b}{(s+\beta_2)} e^{-sT_s} \end{aligned} \tag{16}$$

Transforming Equation (16) into the discrete time domain with consideration of the zero-order-hold (ZOH) effect and then replacing $y(z)$ with $i_i^{\,d}(z)$, $u_c(z)$ with $u_i^d(z)$, and $z_2(z)$ with $z_{2i}^d(z)$ yields the following $G_{zi}(z)$ and $G_{zu}(z)$ in Figure 3:

$$\begin{aligned} G_{zi}(z) &= \frac{z_{2i}^d(z)}{i_i^d(z)} = \left(1 - z^{-1}\right)\mathcal{Z}\left[\mathcal{L}^{-1}\left[\frac{G_{zy}(s)}{s}\right]\right]\Bigg|_{y=i_i^{\,d},\, z_2=z_{2i}^d} = \frac{\omega_0(z-1)}{\left(z-e^{-\omega_0 T_s}\right)} \\ G_{zu}(z) &= \frac{z_{2i}^d(z)}{u_c^d(z)} = \left(1 - z^{-1}\right)\mathcal{Z}\left[\mathcal{L}^{-1}\left[\frac{G_{zu}(s)}{s}\right]\right]\Bigg|_{u_c=u_i^d,\, z_2=z_{2i}^d} = \frac{b\left(1-e^{-\omega_0 T_s}\right)}{z\left(z-e^{-\omega_0 T_s}\right)} \end{aligned} \tag{17}$$

4. Modeling of the Proposed Scheme

In this section, the overall dynamics of the system with the proposed control scheme are modeled. From Figure 3, $z_{2i}^d(z)$ and $u_i^d(z)$ can be expressed as

$$z_{2i}^d(z) = G_{zi}(z)i_i^d(z) - G_{zu}(z)u_i^d(z) \tag{18}$$

$$u_i^d(z) = \frac{K_P\left(i_{iref}^d - i_i^d(z)\right) - z_{2i}^d(z)}{b} \tag{19}$$

By substituting Equations (17) and (18) into Equation (19), we obtain

$$u_i^d(z) = G_1(z)\left(i_{iref}^d - i_i^d(z)\right) - G_2(z)i_i^d(z) \tag{20}$$

where $G_1(z)$ and $G_2(z)$ are defined as follows:

$$\begin{aligned} G_1(z) &= \frac{K_P}{b}\frac{z\left(z-e^{-\omega_0 T_s}\right)}{\left(z^2-e^{-\omega_0 T_s}z-1+e^{-\omega_0 T_s}\right)} \\ G_2(z) &= \frac{\omega_0}{b}\frac{z(z-1)}{\left(z^2-e^{-\omega_0 T_s}z-1+e^{-\omega_0 T_s}\right)} \end{aligned} \tag{21}$$

With a well-tuned RESO, the observer output $z_{2i}^d(z)$ closely tracks the lumped disturbances in the multi-parallel GCIs. The proposed scheme can actively compensate for the effect of lumped disturbances in real time. As indicated by Equation (21), the proposed scheme does not rely on detailed knowledge of the system. The expression for $v_i^d(z)$ from Figure 3 based on Equation (20) are derived as follows:

$$v_i^d(z) = z^{-1}K_{PWM}\Big(G_1(z)\left(i_{iref}^d - i_i^d(z)\right) - G_2(z)i_i^d(z)\Big) \tag{22}$$

Similarly, the expression for $v_j^d(z)$ can be derived as

$$v_j^d(z) = z^{-1}K_{PWM}\Big(G_1(z)\Big(i_{jref}^d - i_j^d(z)\Big) - G_2(z)i_j^d(z)\Big) \tag{23}$$

From Figure 3, the discrete time-domain representation of $i_c{}^d(z)$ can be obtained as

$$i_c^d(z) = \frac{1}{n}G_{coupling}^d(z)\left(v_i^d(z) + \sum_{j=1,j\neq i}^{n} v_j^d(z)\right) \tag{24}$$

By substituting Equations (22) and (23) into Equation (24), $i_c{}^d(z)$ can be expressed as

$$i_c^d(z) = \frac{1}{n}z^{-1}K_{PWM}G_{coupling}^d(z)\left[G_1(z)\sum_{i=1}^{n} i_{iref}^d - (G_1(z)+G_2(z))\sum_{i=1}^{n} i_i^d(z)\right] \tag{25}$$

By applying the current-separation scheme to Figure 3 for considering $i_c{}^d(z)$ only, we obtain

$$\sum_{i=1}^{n} i_i^d(z) = ni_c^d(z) \tag{26}$$

By substituting Equation (26) into Equation (25), the relationship between $i_c{}^d(z)$ and all the current references can be obtained:

$$i_c^d(z) = \frac{1}{n}\cdot\frac{z^{-1}K_{PWM}G_{coupling}^d(z)G_1(z)}{1+z^{-1}K_{PWM}G_{coupling}^d(z)[G_1(z)+G_2(z)]}\sum_{i=1}^{n} i_{iref}^d \tag{27}$$

Similarly, the discrete time-domain representation of $i_{ms}^d(z)$ from Figure 3 can be obtained as

$$i_{ms}^d(z) = \frac{1}{n}G_{plant}^d(z)\left((n-1)v_i^d(z) - \sum_{j=1,j\neq i}^{n} v_j^d(z)\right) \tag{28}$$

By substituting Equations (22) and (23) into Equation (28), $i_{ms}^d(z)$ can be expressed as

$$i_{ms}^d(z) = \frac{1}{n}z^{-1}K_{PWM}G_{plant}^d(z)\left[G_1(z)\sum_{j=1,j\neq i}^{n}\Big(i_{iref}^d - i_{jref}^d\Big) - (G_1(z)+G_2(z))\sum_{j=1,j\neq i}^{n}\Big(i_i^d(z) - i_j^d(z)\Big)\right] \tag{29}$$

The current $i_{ms}^d(z)$ arises only when dissimilar currents exist among inverters; therefore, we obtain

$$\sum_{j=1,j\neq i}^{n}\Big(i_i^d(z) - i_j^d(z)\Big) = n\times i_{ms}^d(z) \tag{30}$$

By substituting Equation (30) into Equation (29), the following expression for $i_{ms}^d(z)$ is obtained:

$$i_{ms}^d(z) = \frac{1}{n}\cdot\frac{z^{-1}K_{PWM}G_{plant}^d(z)G_1(z)}{1+z^{-1}K_{PWM}G_{plant}^d(z)[G_1(z)+G_2(z)]}\sum_{j=1,j\neq i}^{n}\Big(i_{iref}^d - i_{jref}^d\Big) \tag{31}$$

It can be observed from Equation (31) that when $i_{iref}^d = i_{jref}^d$, the mutual current dynamics can be ignored.

By applying the *dq* transformation and discretizing Equation (6), the expression for the current $i_i^d(z)$ can be obtained:

$$i_i^d(z) = i_{ms}^d(z) + i_c^d(z) \tag{32}$$

Substituting Equations (27) and (31) into Equation (32) gives the complete expression of $i_i^d(z)$:

$$\begin{aligned} i_i^d(z) = &\left[\frac{n-1}{n}\frac{z^{-1}K_{PWM}G_{plant}^d(z)G_1(z)}{1+G_{plant}^d(z)[G_1(z)+G_2(z)]} + \frac{1}{n}\frac{z^{-1}K_{PWM}G_{coupling}^d(z)G_1(z)}{1+G_{coupling}^d(z)[G_1(z)+G_2(z)]}\right] i_{iref}^d \\ &+\left[-\frac{1}{n}\frac{z^{-1}K_{PWM}G_{plant}^d(z)G_1(z)}{1+z^{-1}K_{PWM}G_{plant}^d(z)(z)[G_1(z)+G_2(z)]} + \frac{1}{n}\frac{z^{-1}K_{PWM}G_{coupling}^d(z)G_1(z)}{1+z^{-1}K_{PWM}G_{coupling}^d(z)[G_1(z)+G_2(z)]}\right] \sum_{j=1,j\neq i}^{n} i_{jref}^d \end{aligned} \tag{33}$$

The expression in Equation (33) can be simplified by separating the $i_i^d(z)/i_{iref}^d(z)$ and $i_i^d(z)/i_{jref}^d(z)$ characteristics and introducing $T(z)$ and $R(z)$:

$$\begin{aligned} T(z) &= \frac{i_i^d(z)}{i_{iref}^d} = \frac{n-1}{n}\cdot G_{mut}(z) + \frac{1}{n}\cdot G_{com}(z) \\ R(z) &= \frac{i_i^d(z)}{i_{jref}^d} = -\frac{1}{n}\cdot G_{mut}(z) + \frac{1}{n}\cdot G_{com}(z) \end{aligned} \tag{34}$$

where $G_{mut}(z)$ and $G_{com}(z)$ are the two closed-loop transfer functions representing the $i_{ms}^d(z)$ and $i_c^d(z)$, respectively, from Equation (34) and are expressed as

$$\begin{aligned} G_{mut}(z) &= \frac{z^{-1}K_{PWM}G_{plant}^d(z)G_1(z)}{1+z^{-1}K_{PWM}G_{plant}^d(z)[G_1(z)+G_2(z)]} \\ G_{com}(z) &= \frac{z^{-1}K_{PWM}G_{coupling}^d(z)G_1(z)}{1+z^{-1}K_{PWM}G_{coupling}^d(z)[G_1(z)+G_2(z)]} \end{aligned} \tag{35}$$

The performance of the multi-parallel GCIs can be evaluated using Equation (34), which includes $i_{ms}(z)$ and $i_c(z)$ dynamics simultaneously.

5. Resonance Damping and Stability Analysis

The multi-parallel GCIs system is stable if and only if the currents $i_{ms}(z)$ and $i_c(z)$ are stable. From Equation (35), the loop-gain expressions $T_c(z)$ and $T_m(z)$ for the common and mutual current stability, respectively, are obtained as

$$T_c(z) = \frac{z^{-1}K_{PWM}G_{coupling}(z)G_1(z)}{1+z^{-1}K_{PWM}G_{coupling}(z)G_2(z)} \tag{36}$$

and

$$T_m(z) = \frac{z^{-1}K_{PWM}G_{plant}(z)G_1(z)}{1+z^{-1}K_{PWM}G_{plant}(z)G_2(z)} \tag{37}$$

The resonance damping was analyzed via the frequency-response method using Bode plots with different values of n. The stability analysis was performed on the Bode plot by using the Nyquist stability criterion in the frequency range above 0 dB to find the phase margin (PM) of the system above the -180° phase line. Additionally, the gain margin (GM) of the system is measured to determine how much increase in the control bandwidth is possible. The parameters of the proposed control scheme are given in Table 2. The parameter b in the proposed scheme plays an important role in achieving a larger observer bandwidth to improve the disturbance estimation performance of the RESO. A higher value of ω_o can be obtained when a higher value of b is adopted. Generally, ω_o is limited by the sampling frequency f_s [20]. The Bode plot of the loop gain of the mutual current with the proposed scheme is compared with that of conventional derivative filtered capacitor voltage-based active damping using PI control [7] in Figure 4. The corresponding loop-gain expressions for the

conventional scheme are provided in the Appendix A (Equations (A1) and (A2)). The figure indicates that the interactive resonance in the mutual current is independent of the number of parallel inverters. Hence, the frequency response of the mutual current remains the same under different values of n. A small PM of 4° is observed with the conventional scheme owing to the ineffective resonance damping. Additionally, the resonance peak at f_{res} amplifies the resonance, which introduces the mutual current in the parallel GCIs. Moreover, a further increase in the bandwidth of the conventional scheme may violate the system stability. However, the proposed scheme effectively damps the interactive resonance and achieves a larger PM of 69° and a similar crossover frequency as the conventional scheme. With the proposed scheme, no resonance peak is observed above 0 dB at f_{res}, which results in a significantly reduced mutual current in the parallel GCIs.

Table 2. Parameters of RESO-based ADRC current control.

Parameter	Symbol	Value
Gain Parameter	b	$2/L_1$
Observer Bandwidth	ω_o	7 kHz
Proportional Gain	K_p	12,566
PWM Gain	K_{PWM}	~1

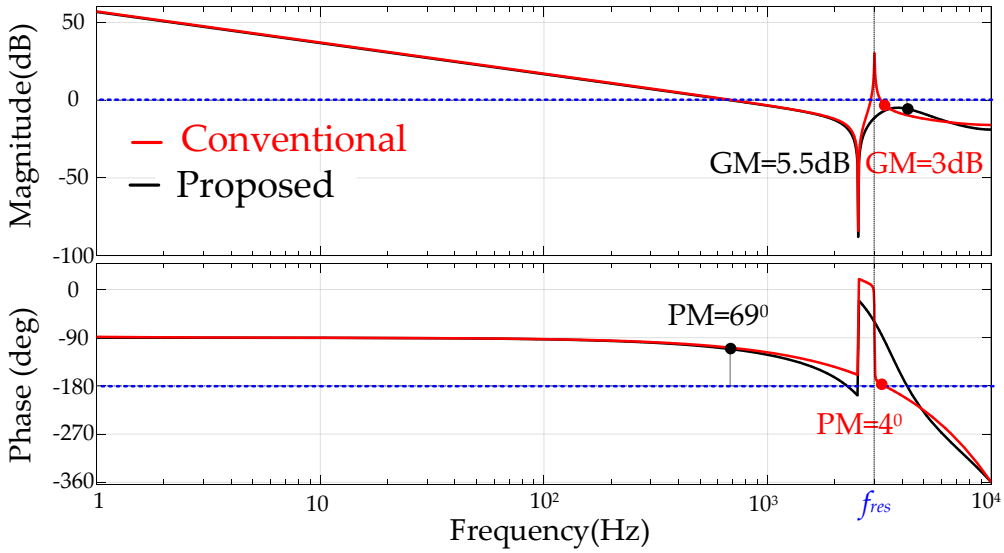

Figure 4. Frequency response of loop gain of mutual current under n = 2, 4, 8, 16, 32 and 64 with the conventional and proposed control scheme.

The frequency response of the loop gain of the common current with the conventional scheme under different values of n is shown in Figure 5. The ω_{res1} is a variable frequency depending on the number of parallel inverters at the PCC; hence, the frequency-response characteristics of the common current are varied according to n. As indicated by the figure, the conventional scheme cannot achieve enough resonance damping, and its disturbance rejection capabilities are highly affected with an increase in the number of inverters. Additionally, only a small PM in the range of 11°–23° is achieved with the conventional scheme, which limits the bandwidth of the control. In contrast, the proposed scheme effectively damps the common resonance regardless of n and maintains a higher stability of the system, disturbance-rejection capabilities, and the crossover frequency of the control, as shown in Figure 6.

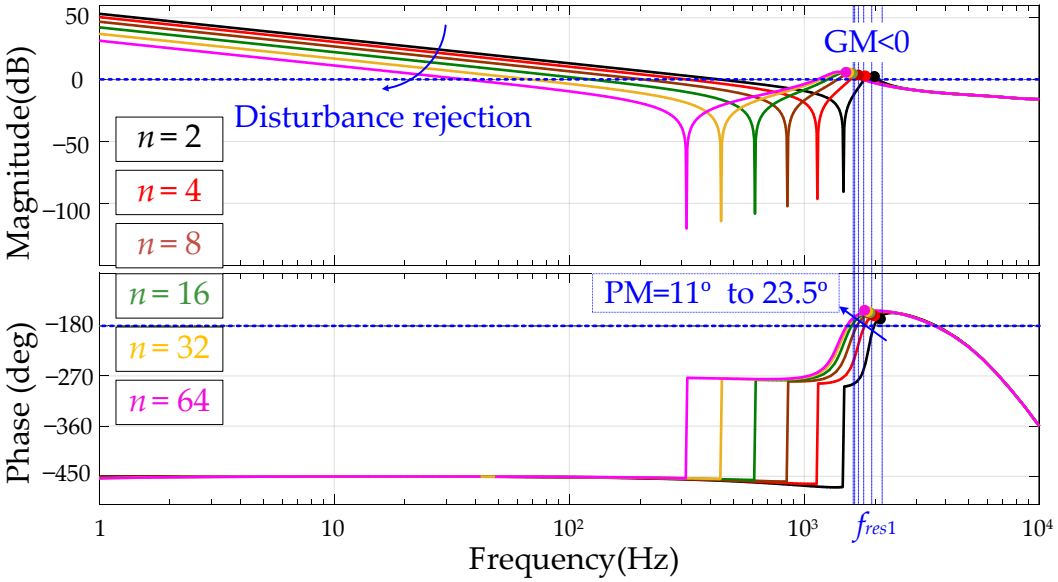

Figure 5. Frequency response of the common current under n = 2, 4, 8, 16, 32 and 64 with the conventional control scheme.

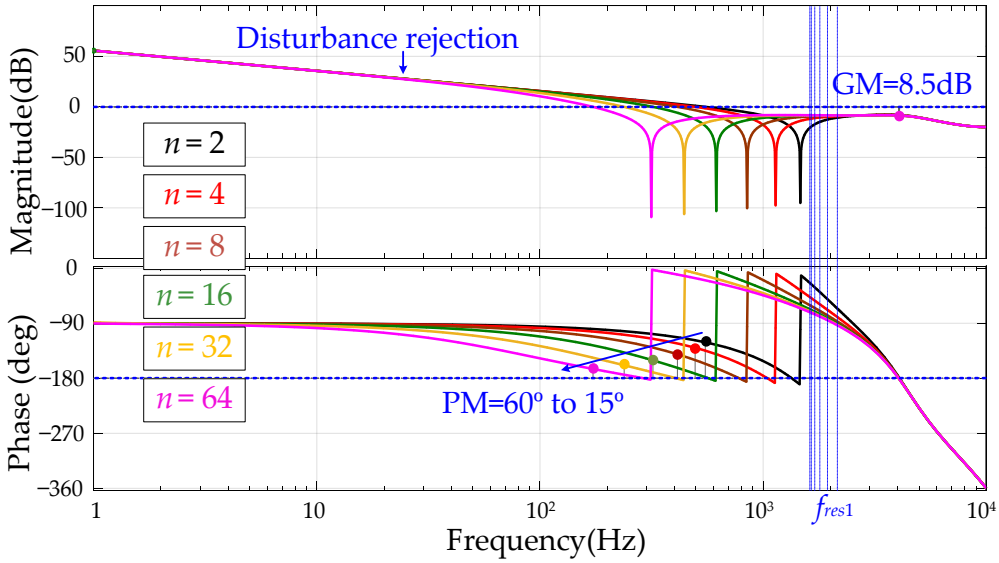

Figure 6. Frequency response of the common current under n = 2, 4, 8, 16, 32 and 64 with the proposed control scheme.

Figure 7a,b show the pole-zero maps of the closed-loop transfer functions $G_{com\_PI}(z)$ and $G_{mut\_PI}(z)$ with the conventional scheme for two parallel GCIs under k_p variation. As shown in Figure 7, the conventional scheme introduces a pole near the unit circle in the common and mutual current, which causes resonance in the system and reduces the stability margin of the system. However, in the pole-zero map of the proposed scheme shown in Figure 8a,b, we observe that the common and interactive resonances are compensated via pole-zero cancelation. Additionally, the common- and mutual-current poles are well inside the unit circle. Hence, the entire system is commonly and mutually stable.

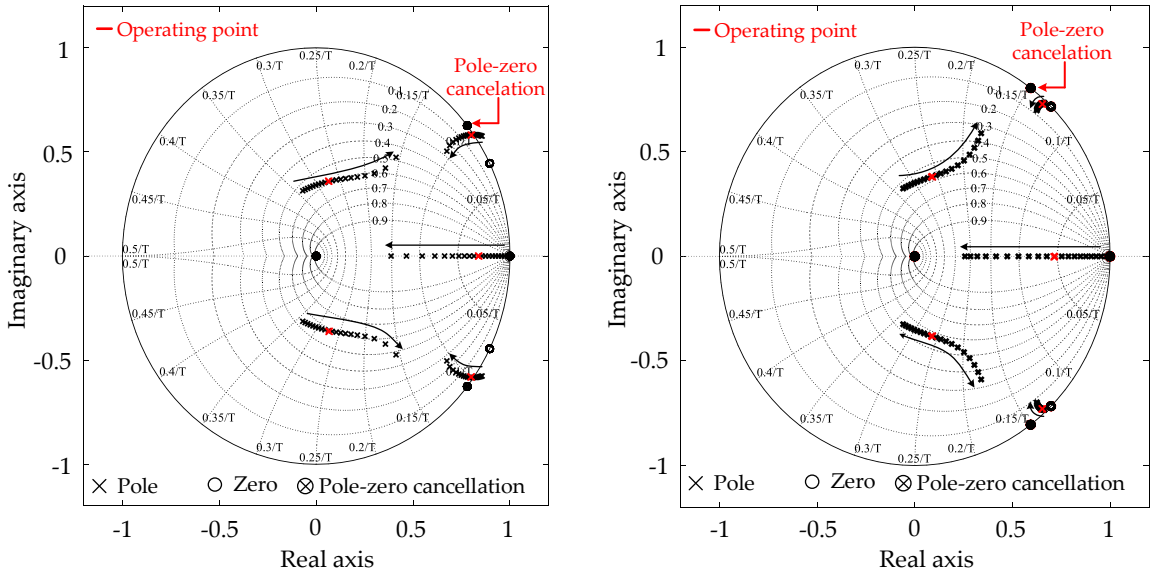

(**a**) Common-current stability (**b**) Mutual-current stability

Figure 7. Pole-zero movement of $G_{com\_PI}(z)$ and $G_{mut\_PI}(z)$ under k_p variation with $n = 2$.

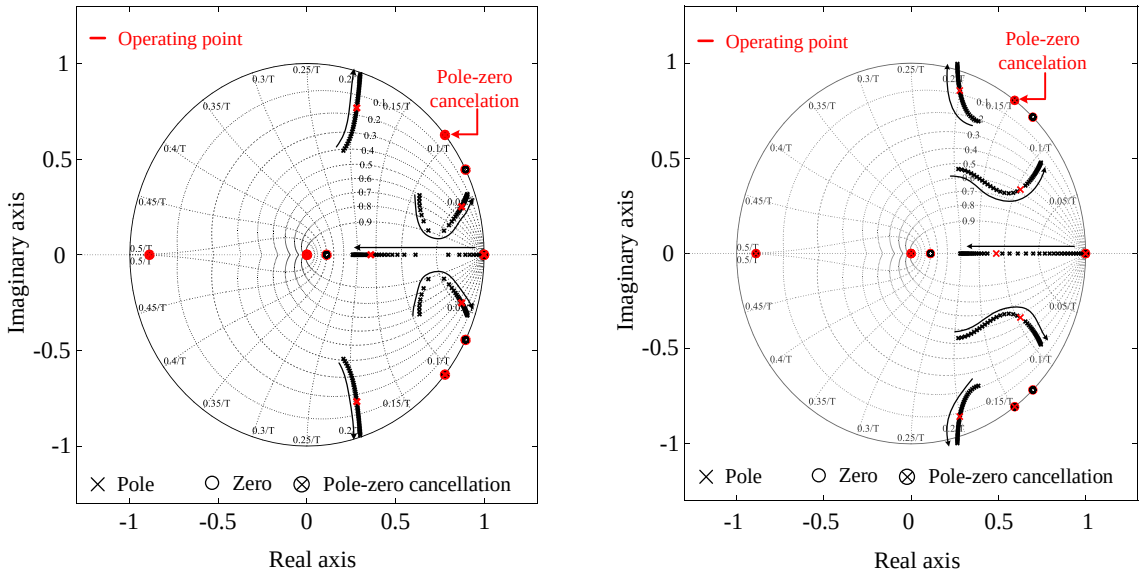

(**a**) Common-current stability (**b**) Mutual current stability

Figure 8. Pole-zero movement of $G_{com}(z)$ and $G_{mut}(z)$ under K_p variation with $n = 2$.

6. Performance Verification

The proposed scheme was verified by simulation and real-time experimental implementation via the HIL technique with a 1 µs step size for the two-parallel GCIs, where the control algorithm was implemented using real-time digital control circuitry.

The performance of the proposed scheme was investigated under two cases: Case I represents the different current references, i.e., $i^d_{1ref} = 5$ A and $i^d_{2ref} = 0$, and Case II represents the same current references, i.e., $i^d_{1ref} = 5$ A and $i^d_{2ref} = 5$ A to each inverter. The current references i^q_{1ref} and i^q_{2ref} to the q-axis current control of inverters #1 and #2 remain zero in both cases.

Figure 9 shows the simulation response of the conventional scheme illustrated in [7]. During Case I, the mutual current is generated in the inverter #2 current, as shown in Figure 9b, owing to the

ineffective interactive resonance damping. Consequently, more resonance harmonics are observed in i_1 and i_c of Figure 9a,c compared with Case II. Additionally, some oscillations during a step change at 20 ms are observed in the common current shown in Figure 9c.

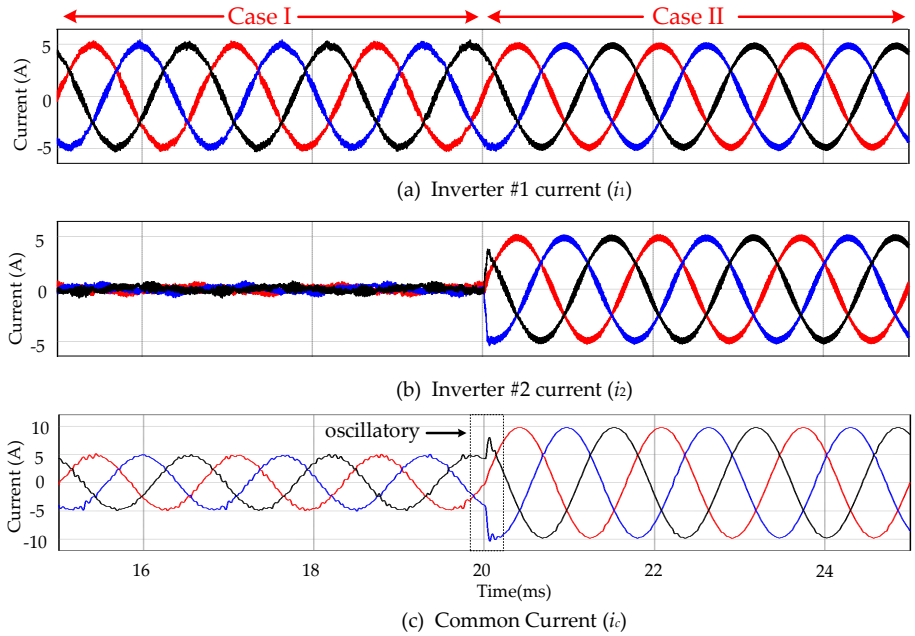

Figure 9. Simulation results for Cases I and II under the conventional scheme presented in [7].

In Figure 10, the simulation responses of the proposed scheme are shown. The proposed scheme effectively damps the common and interactive resonance in Cases I and II. Consequently, no mutual current is observed in the inverter #2 current of Figure 10b. Additionally, no interactive resonance harmonics are observed in i_1 and i_c of Figure 10a,c for both Cases I and II. The smooth tracking response of the common current shown in Figure 11c during a step change at 20 ms explains the larger stability margin, as described in Section 5.

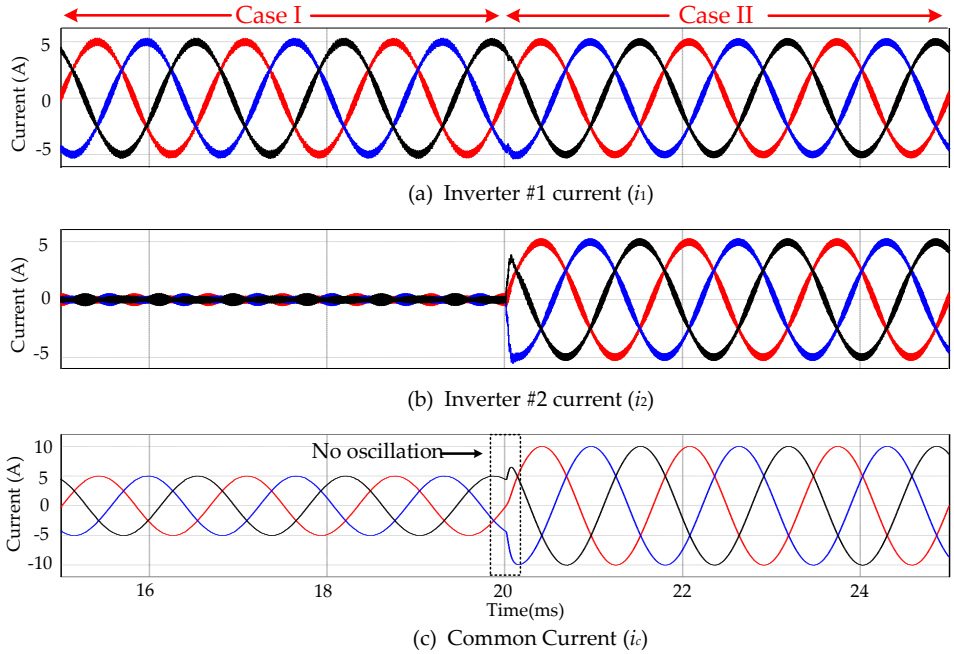

Figure 10. Simulation results for Cases I and II under the proposed scheme.

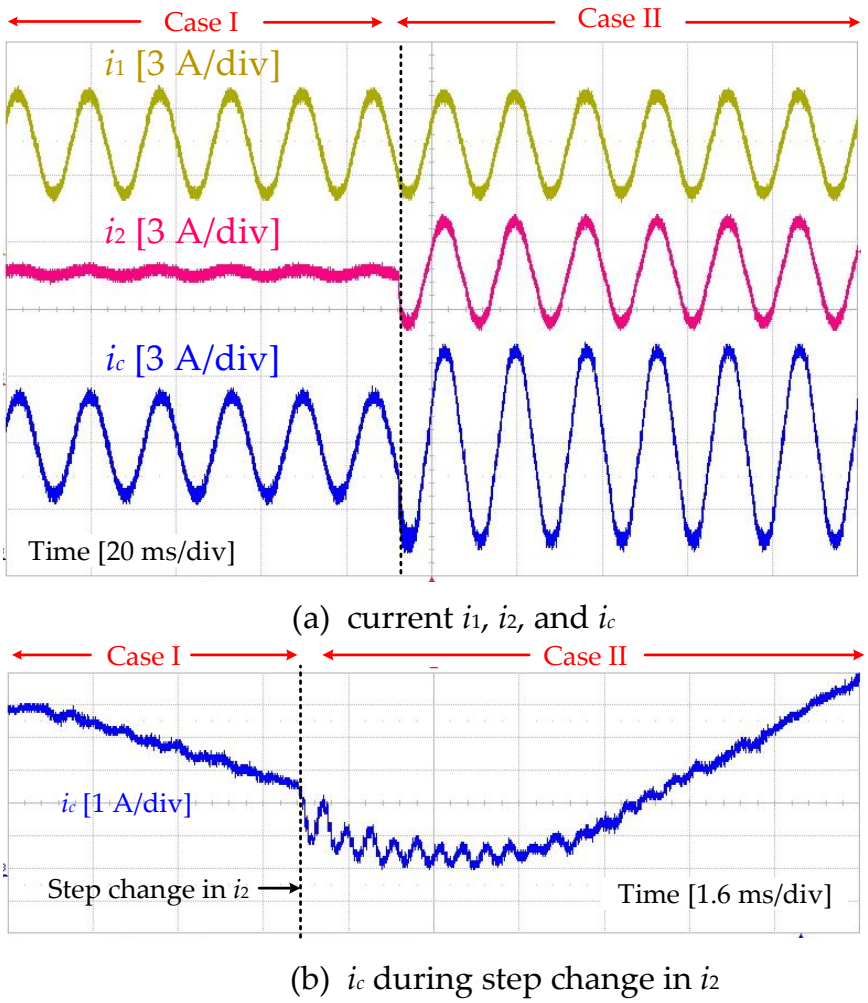

Figure 11. Experimental results for Cases I and II under the conventional scheme presented in [7].

The real-time experimental results of the conventional scheme for Cases I and II are shown in Figure 11. With the adoption of Case I, the mutual current is activated and circulates in inverter #2, as indicated by i_2. The mutual current introduces harmonics in i_1, i_2 and i_c during Case I. During Case II, the mutual current is zero, and interactive resonance harmonics do not exist. Additionally, during the step change in inverter #2 from Case I to II, oscillations in the common current are observed, as shown in Figure 11b, which depicts the simulation performance shown in Figure 10.

The real-time experimental performance of the proposed scheme during Cases I and II is shown in Figure 12. No mutual current is flowing in i_2 when Case I is adopted. In the results, no harmonic oscillation in the steady state is observed in the currents i_1, i_2 and i_c, regardless of the current reference. Additionally, the oscillations in i_c during the step change (from Case I to Case II) are removed, which explains the larger stability margin obtained with the proposed scheme, as shown in Figure 12b. Furthermore, the proposed control scheme achieves robust performance with minimum information about the system required without adopting grid voltage feedforward. This theory can also be applied to a system with an uncertain gird impedance or imbalance v_{pcc}.

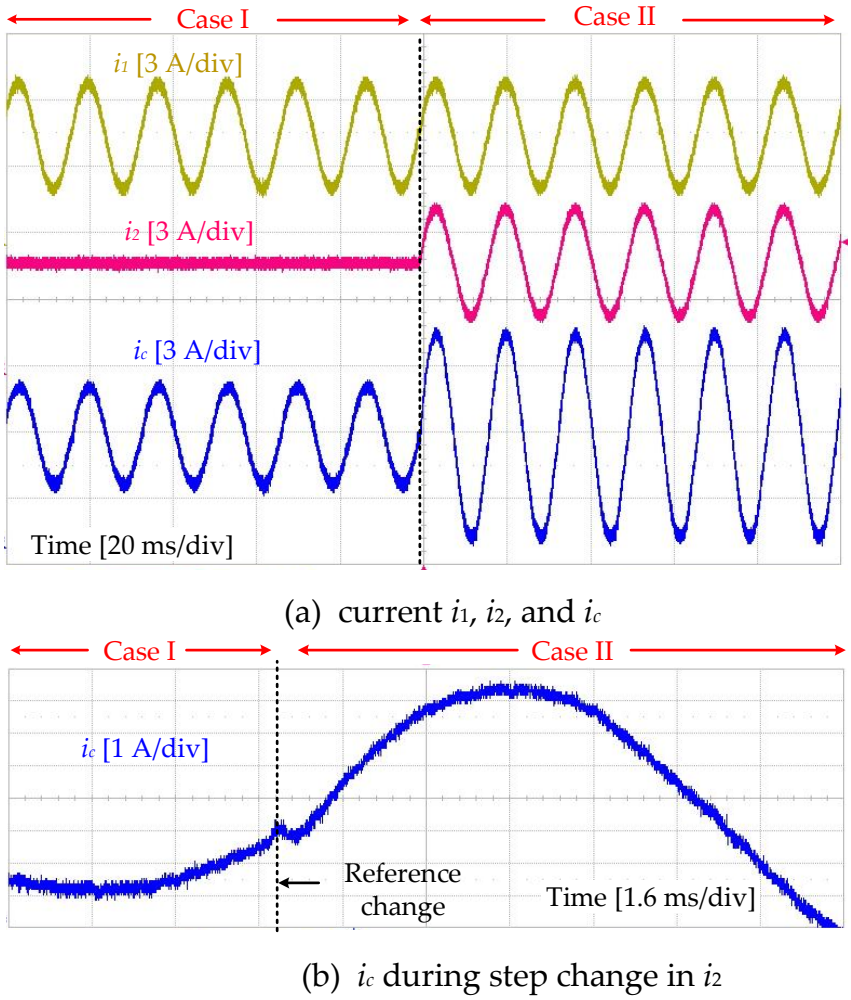

Figure 12. Experimental results for Cases I and II under the proposed control scheme.

The harmonic analysis using the fast Fourier transform (FFT) for the conventional scheme on i_1, i_2 and i_c is shown in Figure 13a,b for Cases I and II, respectively. The resonance is excited in the common current around f_{res} and f_{res1}, which may result in higher THD of i_1 and i_c during Case I, as shown in Figure 13a. The THD of i_1, i_2 and i_c is slightly improved during Case II, as shown in Figure 13b.

The harmonic analysis using the FFT for the proposed scheme on currents i_1, i_2 and i_c is shown in Figure 14a,b for each case. The harmonics around f_{res} and f_{res1} are effectively damped for both Case I and Case II. Additionally, the THD of i_1, i_2 and i_c is greatly improved. During Case I, the THD values for i_1 and i_c measured at the frequency ω_g are calculated as 5.02% and 0.65%, respectively. Similarly, the THD values of i_1, i_2 and i_c during Case II are calculated as 4.84%, 4.84% and 0.20%, respectively.

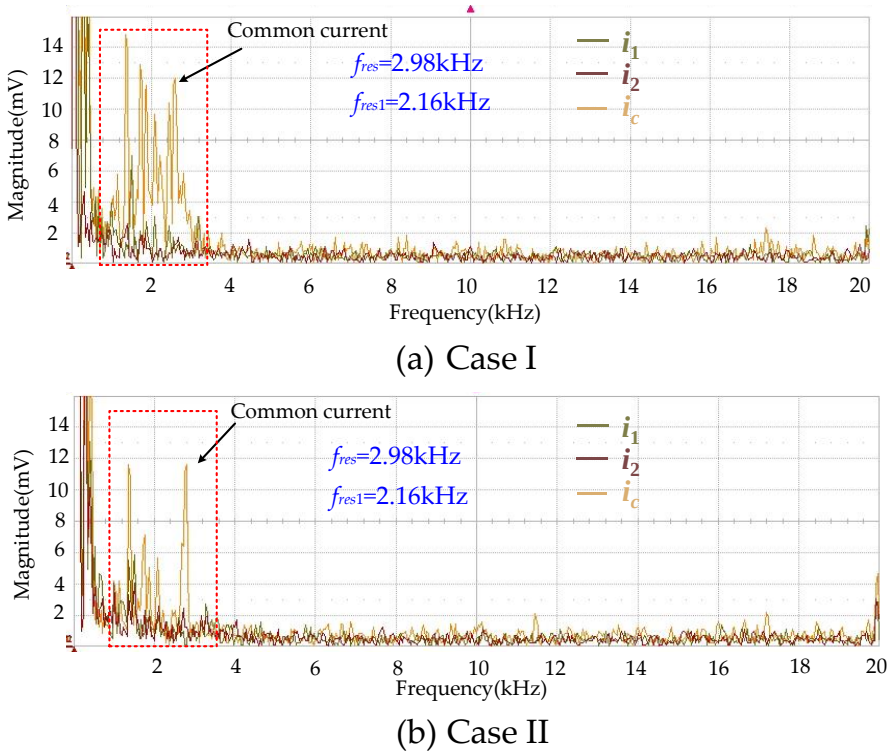

Figure 13. Harmonic analysis under the conventional scheme presented in [7].

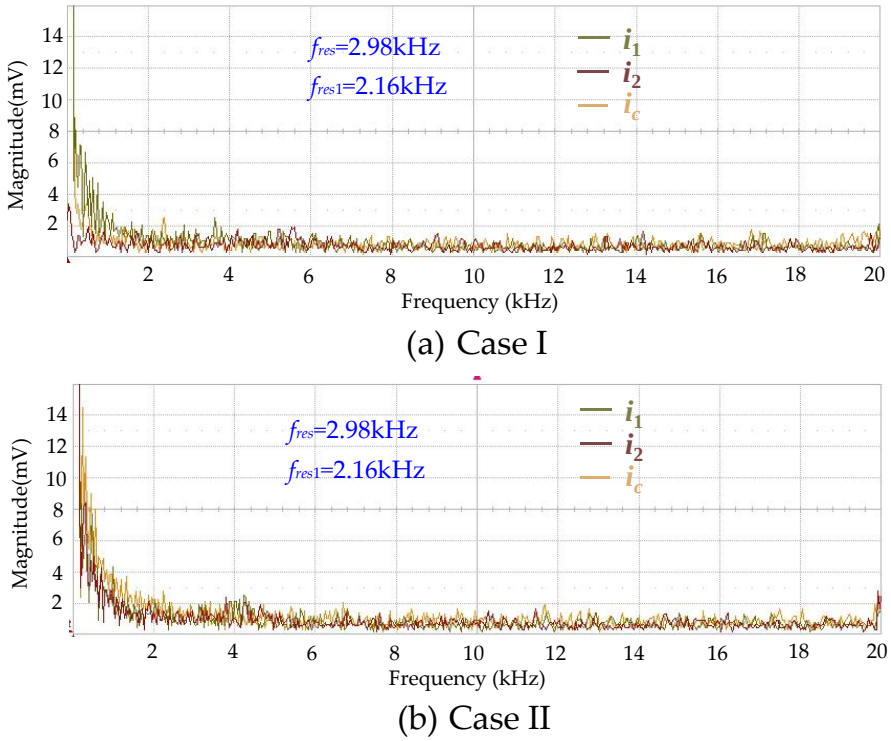

Figure 14. Harmonic analysis under the proposed scheme.

7. Conclusions

An RESO-based ADRC control scheme is proposed for damping the interactive and common resonances present in LCL filter-type three-phase multi-parallel GCIs regardless of the current reference. The proposed scheme treats the interaction among inverters as an exogenous disturbance caused

by other inverters in parallel, estimates it with the RESO, and compensates disturbances in the control law of ADRC. The larger stability margins for the common and mutual current, the preserved disturbance-rejection capabilities under different values of n, and the less model-dependent control design compared to conventional control scheme are the potential benefits of the proposed scheme. The performance of the proposed control scheme was verified and compared with that of the conventional control scheme presented in [7]. A harmonic analysis using the FFT indicates the low THD performance of the proposed method regardless of the current-reference conditions in the system with two parallel GCIs. Thus, the proposed scheme can be extended to a system with an uncertain grid impedance or grid voltage imbalance.

Author Contributions: The individual contribution of each co-author with regards to the reported research writing of the paper is as follows: M.S. conceived the idea, M.S., B.-S.K., S.-H.K. performed the simulation and real-time experimental results. All authors participated in the paper writing.

Funding: This work was supported by "Human Resources Program in Energy Technology" of the Korea Institute of Energy Technology Evaluation and Planning (KETEP), granted financial resource from the Ministry of Trade, Industry & Energy, Republic of Korea. (No. 20184010201710).

Acknowledgments: This work is possible with the support of Higher Education Commission (HEC), Pakistan who supported me financially throughout my journey. I would also like to thank my wife for his moral support.

Conflicts of Interest: The authors declare no conflicts of interest.

Nomenclature

Superscripts	
dq	Quantities in dq reference frame
abc	Quantities in abc reference frame
*	Reference
Subscripts	
n	Number of parallel inverters
i	Inverter number equal to 1, . . . , n
j	Inverter number equal to 1, . . . , n and $j \neq i$
Symbols	
e_g	Grid voltage
V_{pcc}	Voltage at point of common coupling
i_i	Inverter-side current of each inverter
i_{mi}	Mutual current in each inverter
i_c	Common grid flowing into grid
i_{ms}	Mutual current summation
V_i	Inverter-side voltage of each inverter
V_{dci} and C_{dci}	DC-link voltage and capacitance of each inverter
Z_{1i}, Z_{2i} and Z_{3i}	Inverter-side, grid-side and filter capacitance Impedance
Z_g (or L_g)	Grid impedance
L_1, C_3, L_2	Inductive, capacitive and inductive components of LCL filter
Y_{ii} and Y_{ij}	Admittance
G_{plant}	LCL filter transfer function
$G_{coupling}$	Grid coupling transfer function
ω_{res} (or f_{res}) and ω_{res1} (or f_{res1})	Interactive and common resonance frequency
ω_g	Grid fundamental frequency
P_{iref} and Q_{iref}	Active and reactive power reference
i^d_{iref} and i^q_{iref}	Reference of d and q components of current
u_i^{abc}, u_i^{dq}	Control signal in abc and dq reference frame
s_{i1} to s_{i6}	Six pulse gate signals for each IGBT of inverter

b	Gain parameter of ADRC
β_1 and β_2	Observer gains
ω_0	Observer Bandwidth
K_p	Proportional gain of control
T_s	Sampling time
x_1 and x_2	System states
z_{1i} and z_{2i}	Estimated states of ESO
$f(t)$	Lumped disturbances in the system
K_{PWM}	PWM gain
G_{zy}	Output-to-estimation transfer function
G_{zu}	Control-to-estimation transfer function
T_c and T_m	Loop gain expressions for common and mutual current
GM and PM	Gain margin and Phase margin
THD	Total Harmonic Distortion
G_{ad}	Active damping transfer function
G_{vc}	Inverter-side to capacitor voltage transfer function
C_{PI}	PI control transfer function

Appendix A

The loop-gain transfer functions with conventional derivative filtered capacitor voltage-based active damping representing the common and mutual current stability can be expressed as

$$T_{m\_PI}(z) = \frac{z^{-1}K_{PWM}G_{plant}(z)C_{PI}(z)}{1 - z^{-1}K_{PWM}G_{ad}(z)G_{vc1}(z)} \tag{A1}$$

and

$$T_{c\_PI}(z) = \frac{z^{-1}K_{PWM}G_{coupling}(z)C_{PI}(z)}{1 - z^{-1}K_{PWM}G_{ad}(z)G_{vc2}(z)}. \tag{A2}$$

$C_{PI}(s)$ represents the PI control dynamics in the s-domain and is given as

$$C_{PI}(s) = k_p + \frac{k_i}{s}, \tag{A3}$$

where $k_p = \omega_c L_1$ and $k_i = \omega_c(R_1)$.

The transfer functions $G_{vc1}(z)$ and $G_{vc2}(z)$ in Equations (A1) and (A2) relate the inverter-side and LCL filter capacitor voltage as follows:

$$\begin{aligned} G_{vc1}(z) &= \left(1 - z^{-1}\right)\mathcal{Z}\left[\mathcal{L}^{-1}\left[\tfrac{1}{s}\tfrac{1}{L_1C_3}\tfrac{1}{s^2+\omega_{res}^2}\right]\right] \\ G_{vc2}(z) &= \left(1 - z^{-1}\right)\mathcal{Z}\left[\mathcal{L}^{-1}\left[\tfrac{1}{s}\tfrac{1}{L_1C_3}\tfrac{1}{s^2+\omega_{res1}^2}\right]\right] \end{aligned} \tag{A4}$$

The transfer function $G_{ad}(z)$ represents a derivative filtered feedforward term in the capacitor voltage loop calculated in the z-domain as

$$G_{ad}(z) = k_{ad}C_3\frac{1 - z^{-1}}{T_s}. \tag{A5}$$

The closed-loop transfer functions $G_{mut\_PI}(z)$ and $G_{com\_PI}(z)$ representing the mutual and common current can be derived as

$$\begin{aligned} G_{mut\_PI}(z) &= \tfrac{T_{m\_PI}(z)}{1+T_{m\_PI}(z)} \\ G_{com\_PI}(z) &= \tfrac{T_{com\_PI}(z)}{1+T_{com\_PI}(z)} \end{aligned} \tag{A6}$$

References

1. Teodorescu, R.; Liserre, M.; Rodriguez, P. *Grid Converters for Photovoltaic and Wind Power Systems*; John Wiley & Sons: Hoboken, NJ, USA, 2011.
2. Liserre, M.; Teodorescu, R.; Blaabjerg, F. Stability of photovoltaic and wind turbine grid-connected inverters for a large set of grid impedance values. *IEEE Trans. Power Electron.* **2006**, *21*, 263–272. [CrossRef]
3. Wu, W.; Liu, Y.; He, Y.; Chung, H.S.-H.; Liserre, M.; Blaabjerg, F. Damping methods for resonances caused by LCL-filter-based current-controlled grid-tied power inverters: An overview. *IEEE Trans. Ind. Electron.* **2017**, *64*, 7402–7413. [CrossRef]
4. Enslin, J.H.; Heskes, P.J. Harmonic interaction between a large number of distributed power inverters and the distribution network. *IEEE Trans. Power Electron.* **2004**, *19*, 1586–1593. [CrossRef]
5. He, J.; Li, Y.W.; Bosnjak, D.; Harris, B. Investigation and active damping of multiple resonances in a parallel-inverter-based microgrid. *IEEE Trans. Power Electron.* **2013**, *28*, 234–246. [CrossRef]
6. Lu, M.; Wang, X.; Blaabjerg, F.; Loh, P.C. An analysis method for harmonic resonance and stability of multi-paralleled LCL-filtered inverters. In Proceedings of the 2015 IEEE 6th International Symposium on Power Electronics for Distributed Generation Systems 2015, Aachen, Germany, 22–25 June 2015; pp. 1–6.
7. Lu, M.; Wang, X.; Loh, P.C.; Blaabjerg, F. Resonance interaction of multiparallel grid-connected inverters with LCL filter. *IEEE Trans. Power Electron.* **2017**, *32*, 894–899. [CrossRef]
8. Wang, X.; Blaabjerg, F.; Liserre, M.; Chen, Z.; He, J.; Li, Y. An active damper for stabilizing power-electronics-based AC systems. *IEEE Trans. Power Electron.* **2014**, *29*, 3318–3329. [CrossRef]
9. Hong, L.; Shu, W.; Wang, J.; Mian, R. Harmonic resonance investigation of a multi-inverter grid-connected system using resonance modal analysis. *IEEE Trans. Power Del.* **2019**, *34*, 63–72. [CrossRef]
10. Akhavan, A.; Mohammadi, H.R.; Guerrero, J.M. Modeling and design of a multivariable control system for multi-paralleled grid-connected inverters with LCL filter. *Int. J. Electr. Power Energy Syst.* **2018**, *94*, 354–362. [CrossRef]
11. Chen, Z.; Chen, Y.; Guerrero, J.M.; Kuang, H.; Huang, Y.; Zhou, L.; Luo, A. Generalized coupling resonance modeling, analysis, and active damping of multi-parallel inverters in microgrid operating in grid-connected mode. *J. Mod. Power Syst. Clean Energy* **2016**, *4*, 63–75. [CrossRef]
12. Lu, M.; Yang, Y.; Johnson, B.; Blaabjerg, F. An interaction-admittance model for multiple-Inverter grid-connected systems. *IEEE Trans. Power Electron.* **2018**, *34*, 7542–7557. [CrossRef]
13. Qian, Q.; Xie, S.; Huang, L.; Xu, J.; Zhang, Z.; Zhang, B. Harmonic suppression and stability enhancement for parallel multiple grid-connected inverters based on passive inverter output impedance. *IEEE Trans. Ind. Electron.* **2017**, *64*, 7587–7598. [CrossRef]
14. Yu, C.; Zhang, X.; Liu, F.; Li, F.; Xu, H.; Cao, R.; Ni, H. Modeling and resonance analysis of multiparallel inverters system under asynchronous carriers conditions. *IEEE Trans. Power Electron.* **2017**, *32*, 3192–3205. [CrossRef]
15. Cavazzana, F.; Caldognetto, T.; Mattavelli, P.; Corradin, M.; Toigo, I. Analysis of current control interaction of multiple parallel grid-connected inverters. *IEEE Trans. Sustain. Energy* **2018**, *9*, 1740–1749. [CrossRef]
16. Yoon, C.; Bai, H.; Beres, R.N.; Wang, X.; Bak, C.L.; Blaabjerg, F. Harmonic stability assessment for multiparalleled, grid-connected inverters. *IEEE Trans. Sustain. Energy* **2016**, *7*, 1388–1397. [CrossRef]
17. Chen, T.; Lee, C.K.; Hui, R. A general design procedure for multi-parallel modular grid-tied inverters system to prevent common and interactive instability. *IEEE Trans. Power Electron.* **2019**, *34*, 6025–6030. [CrossRef]
18. Chen, W.-H.; Yang, J.; Guo, L.; Li, S. Disturbance-observer-based control and related methods—An overview. *IEEE Trans. Ind. Electron.* **2016**, *63*, 1083–1095. [CrossRef]
19. Wang, B.; Xu, Y.; Shen, Z.; Zou, J.; Li, C.; Liu, H. Current control of grid-connected inverter with LCL filter based on extended-state observer estimations using single sensor and achieving improved robust observation dynamics. *IEEE Trans. Ind. Electron.* **2017**, *64*, 5428–5439. [CrossRef]
20. Wang, B.; Shen, Z.; Liu, H.; Hu, J. Linear ADRC direct current control of grid-connected inverter with LCL filter for both active damping and grid voltage induced current distortion suppression. *IET Power Electron.* **2018**, *11*, 1748–1755. [CrossRef]
21. Benrabah, A.; Xu, D.; Gao, Z. Active disturbance rejection control of LCL-filtered grid-connected inverter using Padé approximation. *IEEE Trans. Ind. Appl.* **2018**, *54*, 6179–6189. [CrossRef]

22. Saleem, M.; Choi, K.-Y.; Kim, R.-Y. Resonance damping for an LCL filter type grid-connected inverter with active disturbance rejection control under grid impedance uncertainty. *Int. J. Electr. Power Energy Syst.* **2019**, *109*, 444–454. [CrossRef]
23. Skogestad, S.; Postlethwaite, I. *Multivariable Feedback Control: Analysis and Design*; Wiley: New York, NY, USA, 2007.
24. Franklin, G.F.; Powell, J.D.; Workman, M.L. *Digital Control of Dynamic Systems*; Addison-Wesley: Menlo Park, CA, USA, 1998.